

A simple model for the charm structure function of nuclei

G.R.Boroun*

Department of Physics, Razi University, Kermanshah 67149, Iran

(Dated: January 10, 2024)

In this paper, we have investigated the importance of quark charm in nuclear structure functions in the color dipole model at small x . The charm structure function per nucleon F_2^{cA}/A for light and heavy nuclei in a wide range of transverse separations \mathbf{r} with renormalization and factorization scales are considered. Bounds on the ratio F_2^{cA}/AF_2^A for nuclei are well described with respect to the electron-ion future colliders kinematic range, i.e, EIC and EIC colliders.

I. Introduction

Electron-nucleus scattering experiments provide vital complementary information to test, assess and validate different nuclear models and data collected from the electron scattering controlled kinematics, large statistics and high precision allow one to constrain nuclear properties and specific interaction processes [1]. The study of nuclear structure function and its modification at small Bjorken x , is a very interesting subject in compared to those for free nucleon observed in deep inelastic scattering (DIS) [2]. For a nucleus A with Z protons and $N = A - Z$ neutrons, the nuclear parton distribution functions (nPDFs) are defined into the parton distribution functions (PDFs) of a bound proton and neutron (i.e., $f_i^{p/A}$ and $f_i^{n/A}$ respectively) by the following form

$$f_i^A(x, Q^2) = \frac{Z}{A} f_i^{p/A}(x, Q^2) + \frac{N}{A} f_i^{n/A}(x, Q^2), \quad (1)$$

where, the bound nucleon PDFs are different from those of a free proton by the nuclear modification factors as

$$R_i^A(x, Q^2) = \frac{f_i^{p/A}(x, Q^2)}{f_i^p(x, Q^2)}. \quad (2)$$

The modification of nuclear structure functions at small Bjorken x in comparison with the free nucleon observed in DIS is defined by small- x shadowing followed by antishadowing and EMC-effect, and at the large- x is Fermi motion. At small values of the Bjorken variable x (for $x < 0.01$), the shadowing effect is seen in nuclear DIS. In the shadowing region, the structure function F_2 per nucleon turns out to be smaller in nuclei than in a free nucleon [3]. This effect manifests itself as an inequality $F_2^A/(AF_2^N) < 1$, where A is the number of nucleons in a nuclear target. Indeed, unitarity driven nuclear shadowing becomes important at $x \ll x_A = 1/(m_N R_A) = 0.15A^{-1/3}$ where R_A is the radius of the target nucleus and m_N is the nucleon mass [4]¹. Nuclear shadowing, in the laboratory frame, derives from the coherent interaction of $q\bar{q}$, $q\bar{q}g$,... states. The Fock state expansion of the physical virtual photon reads $|\gamma^* \rangle = \sqrt{z_g} \Psi_{q\bar{q}} |q\bar{q} \rangle + \Phi_{q\bar{q}g} |q\bar{q}g \rangle$, where $\Psi_{q\bar{q}}$ and $\Phi_{q\bar{q}g}$ are the light-cone wavefunctions of the $q\bar{q}$ and $q\bar{q}g$ states. Here $\sqrt{z_g}$ is the renormalization of the $q\bar{q}g$ state by the virtual radiative corrections for the $q\bar{q}g$ state. For the lowest $|q\bar{q} \rangle$ Fock component of the photon, the interaction of $q\bar{q}$ dipole of transverse separation \mathbf{r} with a nucleon represents with the dipole cross section $\sigma_{q\bar{q}}(r)$ [5,6]. Indeed, the incoming virtual photon splits into a colorless $q\bar{q}$ pair long before reaching the nucleus, and this dipole interacts with typical hadronic cross sections which results in absorption. The key feature is the connection of the dipole-target amplitude to the integrated gluon density where, at very low x , the parton saturation models illuminate the behavior of the gluon density. The dipole cross section can be derived from the Balitsky-Kovchegov (BK) equation [9,10], which established a non-linear evolution equation to describe the high energy scattering of a $q\bar{q}$ dipole on a target in the fixed coupling case based on the concept of saturation. For the study of saturation of nuclei, those have an advantage over protons since they have more gluons to start with. Therefore, non-linear effects in the evolution of the nuclear gluon distribution should set in at much lower energy

*Electronic address: boroun@razi.ac.ir

¹ For further discussion refer to the Refs.[5-8]

than for protons. DIS on heavy nuclei is expected to probe the color dipole cross section in a way different from DIS on nucleons. Specifically, the larger the dipole size is the stronger nuclear screening [11-15]. Unitarity constraints for deep-inelastic scattering on nuclei predicted in Ref.[16]. Evidently, the nuclear shadowing (screening) depends on high mass diffraction.

It is expected that measurements over the extended x and Q^2 ranges, which would become possible for future experiments, in particular, for experiments at the Electron-Ion Collider (EIC) [17] and Electron-Ion Collider in China (EICC) [18], will give more information in order to discriminate between the distinct models of shadowing of the QCD dynamics at small x . These future facilities will probe nuclear structure over a broad range of x and Q^2 and the analysis of the nuclear effects in deep inelastic scattering has been a topic of discussion in the community in recent times². One of the main physics goals of these future QCD laboratories at small x will be to unambiguously unveil the onset of the so-called gluon saturation regime of QCD, which is characterized by a transverse momentum scale, the saturation scale $Q_s(x)$, at which non-linearities become of comparable importance to linear evolution. In the last years the analysis of the nuclear effects in deep inelastic scattering (DIS) has been extensively discussed in the literature [19-31]. In this paper there is a good chance to produce interesting new predictions for the charm structure function of nuclei for future experiments in the low x region. These calculations are based on the color dipole picture (CDP) with a characteristic saturation momentum, Q_s^A . We analyze the charm quark structure functions in nuclei and those ratios in a wide range of r in section II. In this section, the heavy quark structure functions can be combined with the Sudakov form factor. Section III contains our results and conclusions.

II. Method

The cross section in the dipole formulation of the photon-nucleon scattering is defined, with respect to the polarization (transverse, T, or longitudinal, L) of the virtual photon, by

$$\sigma_{L,T}^{\gamma^*p}(x, Q^2) = \int dz d^2\mathbf{r} |\Psi_{L,T}(\mathbf{r}, z, Q^2)|^2 \sigma_{\text{dip}}(x, \mathbf{r}), \quad (3)$$

where $\Psi_{L,T}$ is the corresponding photon wave function in mixed representation and $\sigma_{\text{dip}}(x, r)$ is the dipole cross-section which related to the imaginary part of the $(q\bar{q})p$ forward scattering amplitude. The transverse dipole size r and the longitudinal momentum fraction z due to the photon momentum are defined. The variable z , with $0 \leq z \leq 1$, characterizes the distribution of the momenta between quark and antiquark. The Golec-Biernat and Wusthoff (GBW) model [32] is a model for the so-called dipole cross section, that is used to describe the inclusive DIS data for $x < 0.01$ and all Q^2 . The model reads

$$\sigma_{\text{dip}}(x, r) = \sigma_0 \left\{ 1 - \exp \left[-\frac{1}{4} Q_{\text{sat}}^2 r^2 \right] \right\}, \quad (4)$$

where $Q_{\text{sat}}(x)$ is the saturation scale defined as $Q_{\text{sat}}^2(x) = Q_0^2(x_0/x)^\lambda$ for the proton. Three parameters, σ_0 , λ and x_0 , were determined [33] from a fit to the HERA data and have values, $\sigma_0 = 27.32 \pm 0.35$ mb, $\lambda = 0.248 \pm 0.002$ and $x_0/10^{-4} = 0.42 \pm 0.04$ for the 4-flavor respectively. The fixed parameters are $Q_0^2 = 1$ GeV², $m_u = m_d = m_s = 0.14$ GeV and $m_c = 1.4$ GeV. The quantity x used in expressions above is the modified Bjorken variable, $x = x_{\text{Bj}}(1 + \frac{4m_q^2}{Q^2})$, with m_q being the effective quark mass. This replacing is a simple way to regular the divergence of the cross section. This modification is quite important as heavy quarks contribution are taken into account and implies that the value of the quark mass plays an important role in avoiding the divergence of the cross section.

The Bartels, Golec-Biernat and Kowalski (BGK) model [34], is another phenomenological approach to the color dipole cross section and reads

$$\sigma_{\text{dip}}(x, \mathbf{r}) = \sigma_0 \left\{ 1 - \exp \left(-\frac{\pi^2 r^2 \alpha_s(\mu^2) x g(x, \mu^2)}{3\sigma_0} \right) \right\}. \quad (5)$$

² The center-of-mass energies in electron-ion colliders proposed in China and the US are 15 – 20 GeV for EIC and 30 – 140 GeV for EIC respectively.

The scale μ^2 is connected to the size of the dipole and takes the form $\mu^2 = \frac{C}{r^2} + \mu_0^2$, where the parameters C and μ_0 are determined from a fit to DIS data [33]. Here $g(x, \mu^2)$ is the gluon collinear PDF. In the color transparency domain, $r \rightarrow 0$, the dipole cross section is related to the gluon density by the following form [35]

$$\sigma_{\text{dip}}(x, \mathbf{r}) \simeq \frac{\pi^2 r^2 \alpha_s(\mu^2) x g(x, \mu^2)}{3}. \quad (6)$$

The gluon distribution in the GBW and BGK models take the form

$$xg(x, \mu^2) = \frac{3\sigma_0}{4\pi^2 \alpha_s(\mu^2)} Q_s^2 \quad (7)$$

where α_s is the running coupling at μ^2 scale [36]. The expression for the nuclear gluon distribution $xg^A(x, \mu^2)$ is the same except for the change $Q_s^2 \rightarrow Q_s^{2A}$ with the replacement the area of the target with the coefficient $A^{2/3}$. Therefore, the gluon distribution for a nuclear target with the mass number A is defined by

$$xg^A(x, \mu^2) = \frac{3\sigma_0 A^{2/3}}{4\pi^2 \alpha_s(\mu^2)} Q_s^{2A}, \quad (8)$$

where

$$Q_s^{2A} = Q_s^2 \left(\frac{A\pi R_p^2}{\pi R_A^2} \right)^{\frac{1}{3}} \quad (9)$$

In Ref.[25], it was found $\delta = 0.79 \pm 0.02$ and the nuclear radius is given by the usual parameterization $R_A = (1.12A^{1/3} - 0.86A^{-1/3})$ fm and $\pi R_p^2 = 1.55 \pm 0.02$ fm². The charm structure function in nuclei, owing to the dominance of the gluon distribution, in the collinear generalized double asymptotic scaling (DAS) approach [37] is defined by the following form in the small x region as

$$F_2^{cA}(x, \mu_r^2) \simeq e_c^2 \sum_{n=0} \left(\frac{\alpha_s}{4\pi} \right)^{n+1} B_{2,g}^{(n)}(x, \xi_r) \otimes xg^A(x, \mu_r^2), \quad (10)$$

where $B_{2,g}$ is the collinear Wilson coefficient function in the high energy regime [38] and n denotes the order in running coupling α_s . Here, e_c^2 is the squared charge of the charm and $\xi_r = \frac{m_c^2}{\mu_r^2}$. The default renormalisation and factorization scales are set to be equal $\mu_R^2 = \mu_r^2 + 4m_c^2$ and $\mu_F^2 = \mu_r^2$.

In addition, we consider bounds for F_2^{cA}/F_2^A follows from the standard nuclear dipole picture which gives correlated values in estimate F_L^A/F_2^A into the higher Fock components of the photon wave function. The nuclear structure function F_2^A can be obtained from the γ^*A cross section through the relation

$$F_2^A = Q^2 \sigma^{\gamma^*A} / (4\pi^2 \alpha), \quad (11)$$

where the nuclear cross section is related to the proton cross section by the following form

$$\sigma^{\gamma^*A} \left(\frac{Q^2}{Q_s^{2A}} \right) = \left(\frac{\pi R_A^2}{\pi R_p^2} \right) \sigma^{\gamma^*p} \left(\frac{Q^2}{Q_s^2} \right) \quad (12)$$

where the γ^*p cross section reads [25,28]

$$\sigma^{\gamma^*p} = \bar{\sigma}_0 \left[\gamma_E + \Gamma \left(0, \frac{a(Q_s^{2A})^b}{(Q^2)^b} \right) + \ln \left(\frac{a(Q_s^{2A})^b}{(Q^2)^b} \right) \right]. \quad (13)$$

Here γ_E and $\Gamma(0, \eta)$ are the Euler constant and the incomplete Γ function respectively, where the fit parameters (i.e., a and b) are $a = 1.868$ and $b = 0.746$.

The bound value of F_2^{cA}/F_2^A is obtained by the following form

$$\frac{F_2^{cA}}{AF_2^A} = \frac{4\pi^2 \alpha e_c^2}{Q^2} A^{(\frac{1}{3}-\frac{1}{3})} \left(\frac{\pi R_p^2}{\pi R_A^2} \right)^{(\frac{1}{3}-1)} \frac{\sum_{n=0} (\frac{\alpha_s}{4\pi})^{n+1} B_{2,g}^{(n)}(x, \xi_r) \otimes xg(x, \mu_r^2)}{\bar{\sigma}_0 \left[\gamma_E + \Gamma \left(0, \frac{a(Q_s^{2A})^b}{(Q^2)^b} \right) + \ln \left(\frac{a(Q_s^{2A})^b}{(Q^2)^b} \right) \right]} \quad (14)$$

which will be interesting in EIC and EICc colliders in the future energy range. Especially at the EIC, it is expected to be probed at an essentially low x (up to $x \sim 10^{-4}$), thus providing us with new information on the charm quark density in a nuclei. Indeed, both EIC in the small- x region and EICc at moderate x give us nuclear modification of the structure functions and hadron production in deep inelastic scattering eA collisions and new information on the parton distribution in nuclei [38].

III. Numerical Results

In the present paper we consider the charm structure function of the deep inelastic scattering of nuclei, which is directly related with the gluon distribution of nuclei in the CDP approach at low x . In this model, the ratios $xg^A(x, \mu^2)/Axg(x, \mu^2)$ and $F_2^{cA}(x, \mu_r^2)/AF_2^c(x, \mu_r^2)$ are independent of the variables and depend on the mass number A by the following form

$$R^A \equiv \frac{F_2^{cA}(x, \mu_r^2)}{AF_2^c(x, \mu_r^2)} \propto \frac{xg^A(x, \mu^2)}{Axg(x, \mu^2)} = A^{-1/3} \left(\frac{A\pi R_p^2}{\pi R_A^2} \right)^{\frac{1}{5}} \quad (15)$$

which gives a plateau behavior in the region $x \leq 0.01$, which is similar with the results F_2^A/AF_2 in Refs.[25,28]. In Fig.1, we plot this ratio for a wide range of A and observe that this ratio is independent of x and r . We observe that the ratio of R^A rapid drop for $A < 50$ followed by a slow rise for larger A . The minimum values of the ratio are found around $A \approx 56$ where these nuclei are the most tightly bound [39]. The increase of binding energy to $A \approx 56$ decreases the momentum carried by parton distributions in comparison with other nuclei.

Our numerical results for charm structure functions of nuclei per nucleon, F_2^{cA}/A are shown in Fig.2 into the

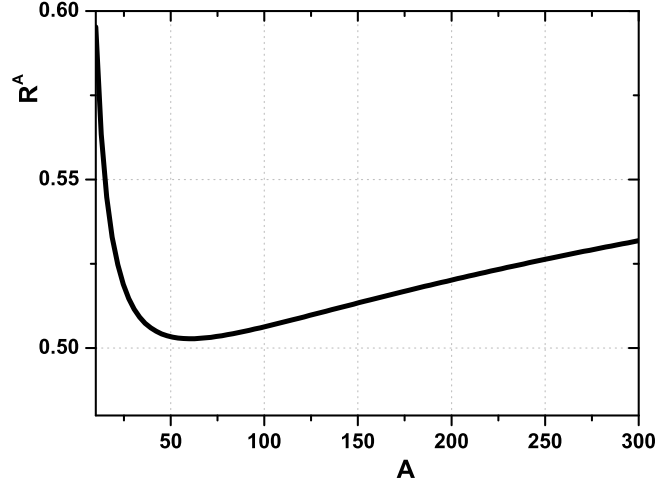


FIG. 1: The ratios $xg^A(x, \mu^2)/Axg(x, \mu^2)$ and $F_2^{cA}(x, \mu_r^2)/AF_2^c(x, \mu_r^2)$ into the mass number A .

uncertainties of the renormalization and factorization scales in a wide range of r for $x = 0.0013$ and 0.0130 . These

TABLE I: The transverse separation range of r in the future facilities(i.e., EIC and EIC) with the inelasticity $y \leq 1$ for $x = 0.0013$ and 0.0130 .

Collider	$\sqrt{s_{\max.}}$ [GeV]	$x=0.0013$	$x=0.0130$
EIC	140	$r > 0.1$	$r > 0.03$
EIC	20	—	$r > 0.3$

results for F_2^{cA}/A , in Fig.2, increase as r decreases for light and heavy nuclei. We observe that the results of F_2^{cA}/A for light and heavy nuclei, at very low r , will increase at the EIC according to the kinematic coverage of the deep inelastic scattering process. The uncertainties due to the renormalization and factorization scales increase as r increase. Owing to the $x - Q^2$ EIC kinematics³, the new information on the charm structure function in nuclei can

³ Please see Fig.1.7 in Ref.[40].

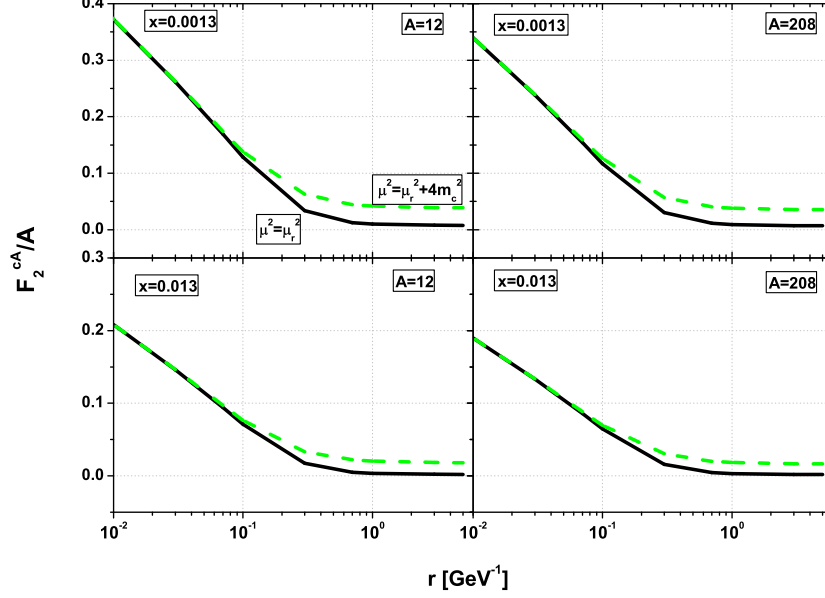


FIG. 2: Results of the charm structure function per nucleon F_2^{cA}/A for light and heavy nuclei in a wide range of the transverse separation $r[\text{GeV}^{-1}]$ with $x = 0.0013$ and $x = 0.0130$. The uncertainties are due to $\mu^2 = \mu_r^2 + 4m_c^2$ (dashed lines) and $\mu^2 = \mu_r^2$ (solid lines).

be achieved with $x = 0.0130$ for $r \gtrsim 0.06 \text{ GeV}^{-1}$ and with $x = 0.0013$ for $r \gtrsim 0.2 \text{ GeV}^{-1}$. As a result, we predict that at low r , the charm structure function will increase at the EIC than the EIC at high inelasticity according to Table I. In Figs.3 and 4, we plot the ratio F_2^{cA}/AF_2^A for nuclei $A = 12$ and $A = 208$, respectively, as a function of r with

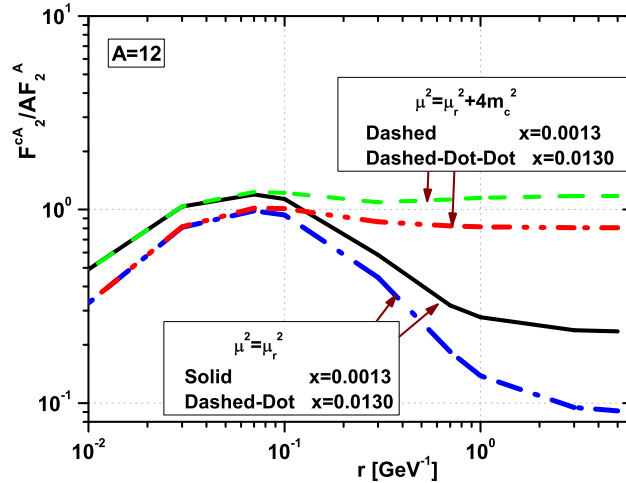


FIG. 3: F_2^{cA}/AF_2^A evaluated as a function of r with $\mu^2 = \mu_r^2 + 4m_c^2$ and $\mu^2 = \mu_r^2$ for nuclei $A=12$ at $x = 0.0013$ and $x = 0.0130$.

the renormalization and factorization scales with $x = 0.0013$ and $x = 0.0130$. These results in Figs.3 and 4 are shown a flat behavior of F_2^{cA}/AF_2^A with $\mu^2 = \mu_r^2 + 4m_c^2$ and decrease sharply with $\mu^2 = \mu_r^2$ at $r \gtrsim 10^{-1} \text{ GeV}^{-1}$. The renormalization and factorization scales results for light and heavy nuclei are compatible at $r < 10^{-1} \text{ GeV}^{-1}$

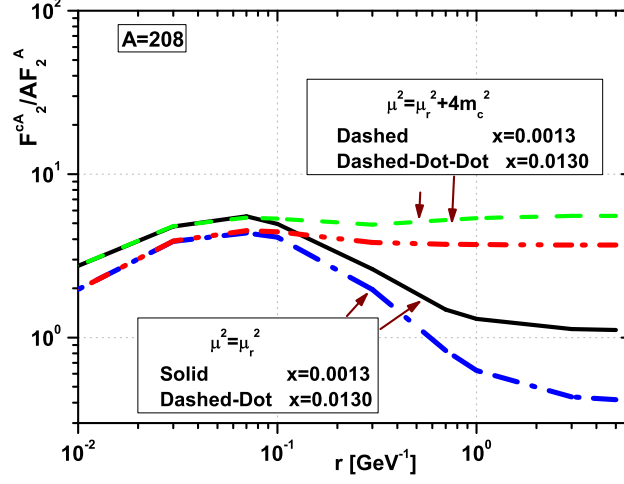


FIG. 4: The same as Fig.3 for A=208.

and have the largest uncertainties at $r > 10^{-1} \text{ GeV}^{-1}$. The maximum value of F_2^{cA}/AF_2^A , in accordance to the EIC kinematic range, is $\simeq 1.3$ and 5.5 for nuclei $A = 12$ and $A = 208$ respectively. Indeed, the importance of the nuclear structure function ratios will depend on the values of F_2^{cA}/AF_2^A , where these bounds can further restrict the kinematical range of the applicability of the dipole picture in the future electron-ion colliders (i.e., EIC and EIC).

Summarizing, a simple model for the charm structure functions in nuclei, in the region of small x , has been presented. We analyzed F_2^{cA} using the gluon density from the GBW and BGK models, inspired by the DAS approach, within the color dipole model to the future electron-ion colliders kinematic range at EIC and EIC, in a wide range of transverse separations r . Our results indicate that the study of the charm structure functions in the eA process at EIC is ideal for considering the heavy quark effects present in the nuclear structure functions, which, in turn, is a crucial ingredient to estimate the bounds of the processes which will be studied in future accelerators. We have considered the charm structure function F_2^{cA}/A per nucleon in light and heavy nuclei, then have obtained bounds on F_2^{cA}/AF_2^A at moderate and large r with the renormalization and factorization scales. We demonstrated the importance of the contributions of F_2^{cA}/A and F_2^{cA}/AF_2^A at small r in the EIC and EIC colliders. The uncertainties of these results are due to the standard variations in the renormalization and factorization scales which increase as r increases. The focus of this paper was to provide an analytical charm structure function per nucleon in nuclei for studying high energy lepton-nucleus phenomena at future colliders such as EIC and the EIC.

ACKNOWLEDGMENTS

The author is grateful to Razi University for the financial support of this project. Thanks is due to N.N.Nikolaev for useful discussions.

REFERENCES

1. V.Pandey, Phys.Sci.Forum **8**, 1 (2023).
2. European Muon, J. Aubert et al., Phys.Lett.B **123**, 275 (1983).
3. P.Paakkinen, arXiv [hep-ph]: 1802.05927.
4. N.N.Nikolaev and V.I.Zakharov, Phys.Lett.B **55B**, 397 (1975); N.N.Nikolaev, W.Schafer, B.G.Zakharov and V.R.Zoller, J.Exp.Theor.Phys.**97**, 441 (2003).

5. M. Krelina and J.Nemchik, Eur.Phys.J.Plus **135**, 444 (2020).
6. N.N.Nikolaev, W.Schafer, B.G.Zakharov and V.R.Zoller, J.Exp.Theor.Phys.Letters **84**, 537 (2006).
7. J.L.Albacete, N.Armento, A.Capella, A.B.Kaidalov and C.A.Salgado, arXiv[hep-ph]:0308050, Report number: CERN-TH/2003-184.
8. L.S.Moriggi, G.M.Peccini and M.V.T.Machado, Phys.Rev.D **103**, 034025 (2021).
9. Y.V.Kovchegov, Phys.Rev.D **60**, 034008 (1999); Phys.Rev.D **61**, 074018 (2000).
10. I.Balitsky, Nucl.Phys.B **463**, 99 (1996); Phys.Lett.B **518**, 235 (2001).
11. D.A.Fagundes and M.V.T.Machado, Phys.Rev.D **107**, 014004 (2023).
12. Qing-Dong Wu et al., Chin.Phys.Lett. **33**, 012502 (2016).
13. M.Genovese, N.N.Nikolaev and B.G.Zakharov, J.Exp.Theor.Phys. **81**, 633 (1995).
14. I.P.Ivanov, N.N.Nikolaev, Phys.Rev.D **65**, 054004 (2002).
15. N.N.Nikolaev and V.R.Zoller, Phys.Lett.B **509**, 283 (2001).
16. N.N.Nikolaev, W.Schafer, B.G.Zakharov and V.R. Zoller, J.Exp.Theor.Phys. Letters **84**, 537 (2007).
17. A.Accardi et al., Eur.Phys.J.A **52**, 268 (2016).
18. D.P.Anderle et al., "Electron-Ion Collider in China," Frontiers of Physics **16**, 64701 (2021).
19. J.Rausch, V.Guzey and M.Klasen, Phys.Rev.D **107**, 054003 (2023).
20. H.Khanpour and S.Atashbar Tehrani, Phys.Rev.D **93**, 014026 (2016).
21. H.Khanpour et al., Phys.Rev.D **104**, 034010 (2021).
22. G.R.Boroun and B.Rezaei, arXiv:2303.07654; G.R.Boroun, B.Rezaei and F.Abdi, arXiv:2305.01893.
23. F.Carvalho, F.O.Duraes, F.S.Navarra and S.Szpigel, Phys.Rev.C **79**, 035211 (2009).
24. J.Raufeisen, Acta Phys.Polon. B **36**, 235 (2005).
25. Nestor Armento, Carlos A. Salgado, Urs Achim Wiedemann, Phys.Rev.Lett. **94**, 022002 (2005).
26. N.Armento, Eur.Phys.J.C **26**, 35 (2002).
27. C.Marquet, Manoel R.Moldes and P.Zurita, Phys.Lett.B **772**, 607 (2017).
28. M.A.Betemps and M.V.T.Machado, Eur.Phys.J.C **65**, 427 (2010).
29. E.R.Cazaroto, F.Carvalho, V.P.Goncalves and F.S.Navarra, Phys.Lett.B **671**, 233(2009).
30. F.Muhammadi and B.Rezaei, Phys.Rev.C **106**, 025203 (2022).
31. N.Armento, C.Merino, G.Parente and E.Zas, Phys.Rev.D **77**, 013001 (2008).
32. K.Golec-Biernat and M.Wusthoff, Phys.Rev.D **59**, 014017 (1998); Phys.Rev.D **60** 114023 (1999).
33. K. Golec-Biernat and S.Sapeta, J.High Energy Phys. **03**, 102 (2018).
34. J.Bartels, K.Golec-Biernat and H.Kowalski, Phys. Rev. D**66**, 014001 (2002).
35. B.Blaettel, G.Baym, L.L.Frankfurt and M.Strikman, Phys.Rev.Lett. **70**, 896 (1993); L.Frankfurt, A.Radyushkin and M.Strikman, Phys.Rev.D **55**, 98 (1997).
36. G.R.Boroun and B.Rezaei, arXiv:2309.04832.
37. A.V.Kotikov, A.V.Lipatov and P.Zhang, Phys.Rev.D **104**, 054042 (2021).
38. J.L.Albacete, N.Armento, J.G.Milhano, C.A.Salgado, and U.A.Wiedemann, Eur.Phys.J.C **43**, 353 (2005).
39. Samuel S.M.Wong, Introductory Nuclear Physics, Prentice-Hall of India Private Limited (2007).
40. D.P.Anderle et al., Front.Phys. **16**, 64701 (2021).